

Analysis of Two Beam Interference Fringes Crossing Graded Index Optical Fibers Using Phase-Shifting Technique

R. M. El-Agmy*, A. E. Elmahdy, A. M. Abd-Rabou and G. M. A. Gad

Helwan University, Faculty of Science, Physics department, 11792 Ain Helwan- Cairo, Egypt.

Received: 4 Jul. 2016, Revised: 10 Oct. 2016, Accepted: 15 Oct. 2016.

Published online: 1 Jan. 2017.

Abstract: A mathematical expression for two-beam interference fringes crossing graded-index (GRIN) optical fiber is derived. The derived model determines the integrated optical path crossing the core of the GRIN optical fiber. The numerical evolution of the model at different values of the fiber exponent optical parameter α is discussed. The theoretical calculations are verified experimentally using high precision phase-shifting interferometry (PSI). The main advantage of the derived model leads to accurate determination of the propagation optical parameters of GRIN optical fibers.

Keywords: Fiber, two beam interference, GRIN

1 Introduction

With the pride advancement of optical fiber communications, a variety of fiber designs have been proposed and employed in various applications due to their specific advantages even active fibers with core doped rare-earth ions [1-6]. These include step-index and graded-index (GRIN) optical fibers. The development of GRIN optical fibers is of great interest since it solved the limitation of transmission data rate in step-index optical fibers [7-9].

In GRIN optical fibers, the core refractive index continually decreases (as a gradient), starting from the fiber core center towards the fiber cladding. A versatile core refractive-index profile $n_c(r)$ is a function of radial position (r) measured from the fiber centre and is described as the power-law function [9]:

$$n_c^2(r) = n_0^2 \cdot \left[1 - 2 \cdot \Delta \cdot \left(\frac{r}{r_c} \right)^\alpha \right], r \leq r_c$$

$$, \text{ with, } \Delta = \frac{n_0^2 - n_{cl}^2}{2n_0^2} \approx \frac{n_0 - n_{cl}}{n_0} \quad (1)$$

where (n_{cl}) is the cladding refractive index, (n_0) is the core refractive index at the centre and (r_c) is the core radius. The parameter α - is the profile exponent or the steepness of the profile. The refractive index $n_c^2(r)$ is a linear function of (r) at $\alpha = 1$ and a quadratic function for $\alpha = 2$. The quantity $n_c^2(r)$ becomes increasingly steep as α becomes larger, and ultimately approaches a step function for $\alpha \rightarrow \infty$ (step-index fiber). However, various index profile defects of

fiber preform (centre defects as tips and dips, deviation of power-law parameter α from optimum value of 2 [10], can significantly reduce the bandwidth and, hence, degrade the desired function of GRIN optical fibers [10]. Therefore, adjustments of the refractive index profiles, core diameter are major of interest during and after manufacturing processes. Common non-destructive traditional interferometric techniques like two-beam as well as multiple-beam methods were used intensively to determine the optical properties of fibrous material [11-14].

Recently, phase shifting interferometry (PSI) [15, 16] and phase shifting digital holographic microscopic interferometry [17-20], in combination with the multilayer theoretical model [21], was employed to characterize the optical properties of GRIN optical fibers. The model [21] has considered and approximated the core of the GRIN optical fiber to circular step-index multilayers optical fiber. Accordingly, inhomogeneity in each layer is added to each other and resulting in discontinuity in the refractive index profile. The integration of the optical path across the fiber core of varying refractive index is the exact solution to avoid the discontinuity in the refractive index profile.

In this work, is derived a new mathematical expression for two-beam interference fringes crossing graded-index GRIN optical fibers. The derived model determines the integrated optical path crossing the core of the GRIN optical fiber. The presented mathematical calculations allow an accurate determination of the optical parameters of GRIN optical fiber. The theoretical calculations were validated experimentally using high precision phase-shifting interferometry.

*Corresponding author e-mail: Redaagmy@science.helwan.edu.eg

2 Theoretical analysis of GRIN optical fibers

Consider a GRIN optical fiber of radius r_f and core radius r_c . The fiber is immersed in a liquid cell of thickness t and filled with a liquid of refractive index n_L . The cell is introduced in one arm of Mach-Zehnder interferometer and illuminated with monochromatic light of wavelength λ as shown in (Fig. 1-a).

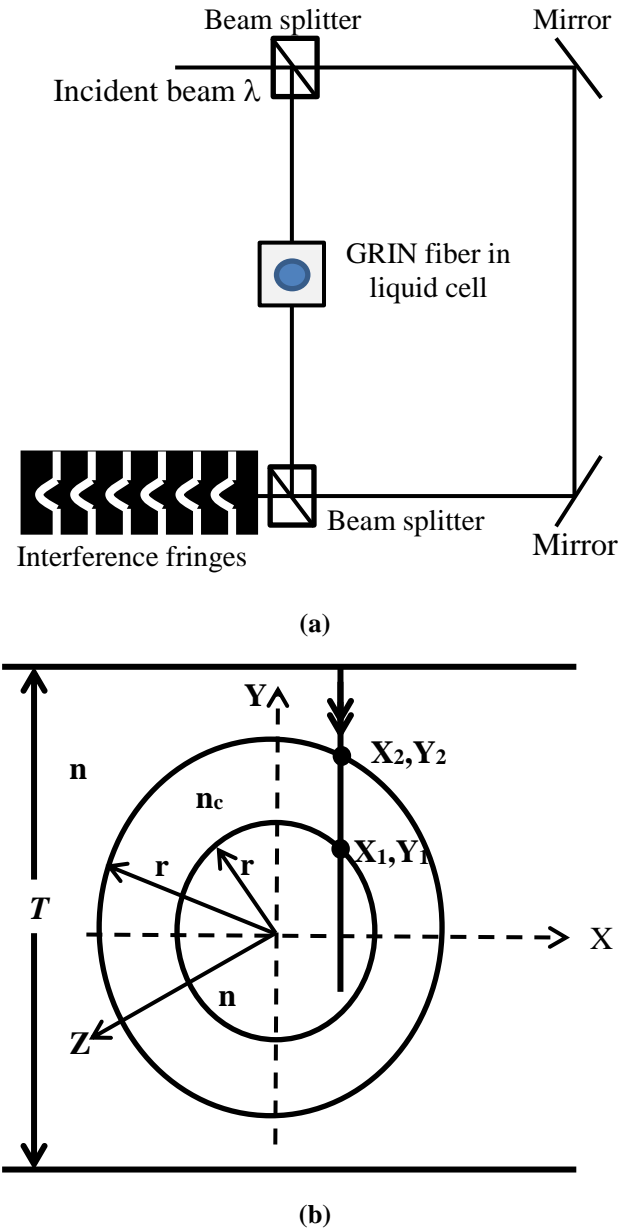


Fig. 1. (a) Schematic diagram of Mach-Zehnder interferometer with a liquid cell containing GRIN optical fiber in one of its arms. (b) Cross section of the liquid cell and GRIN optical fiber, where the light beam crosses the fiber along the Y-axis.

Taking into consideration the same concept of the wedge interferometer to obtain straight lines interference pattern,

one of the Mach-Zehnder mirrors should be tilted with respect to the others. The light beam traverses the fiber parallel to the Y-axis of X-Y plane representing the fiber cross section. The Z-axis is along the fiber length, as shown in (Fig. 1-b). The change in the optical path length (δOPL) of a beam crossing the fiber with respect to the reference one is given by:

$$\delta OPL = 2y_2(n_{cl} - n_L) + 2y_1(n_c(r) - n_{cl}) \quad (2)$$

Where $y_1 = \sqrt{r_c^2 - x^2}$, $y_2 = \sqrt{r_f^2 - x^2}$ and the radial distribution of the core refractive index $n_c(r)$ is given by:

$$n_c(r) = n_0 \left[1 - \Delta \left(\frac{r}{r_c} \right)^\alpha \right] \quad \text{for } r < r_c \quad (3)$$

and

$$\Delta = \frac{n_0 - n_{cl}}{n_0}$$

where n_0 is the refractive index at the fiber center, and α is the exponential order of the refractive index profile and acts as profile shape parameter.

The δOPL corresponds to phase change $\left(\frac{2\pi}{\lambda} \delta OPL \right)$ and in turn fringe shift dZ along the Z-axis. The fringe spacing (ΔZ), not crossing the fiber, corresponds to phase change 2π . Thus the ratio between the fringe shift (dZ) to the fringe spacing (ΔZ) is given by:

$$\frac{\lambda dZ}{2 \Delta Z} = y_2(n_{cl} - n_L) - y_1 n_{cl} + \int_0^{\sqrt{r_c^2 - x^2}} n_c(r) dy \quad (4)$$

Substituting for the values of y_1 and y_2 into eq. (4), one gets:

$$\frac{\lambda dZ}{2 \Delta Z} = (n_{cl} - n_L) \sqrt{r_f^2 - x^2} - n_{cl} \sqrt{r_c^2 - x^2} + \int_0^{\sqrt{r_c^2 - x^2}} n_c(r) dy \quad (5)$$

The last term in eq. (5) can be calculated as follows:

$$\int_0^{\sqrt{r_c^2 - x^2}} n_c(r) dy = \int_0^{\sqrt{r_c^2 - x^2}} n_0 \left[1 - \Delta \left(\frac{r}{r_c} \right)^\alpha \right] dy$$

Where $r = \sqrt{x^2 + y^2}$, then integrate with respect to y , we obtain:

$$\int_0^{\sqrt{r_c^2 - x^2}} n_0 \left[1 - \Delta \left(\frac{r}{r_c} \right)^\alpha \right] dy = n_0 \sqrt{r_c^2 - x^2} - \frac{n_0 \Delta}{r_c^\alpha} \int_0^{\sqrt{r_c^2 - x^2}} (x^2 + y^2)^{\frac{\alpha}{2}} dy \quad (6)$$

The integration of the last term in eq. (6) which is given by:

$$I = \frac{n_0 \Delta}{r_c^\alpha} \int_0^{\sqrt{r_c^2 - x^2}} (x^2 + y^2)^{\frac{\alpha}{2}} dy \quad (7)$$

Eq. (7) can be integrated by substituting $y = x \tan \theta$, then $dy = x \sec^2 \theta d\theta$ and

$$\begin{aligned} \theta &= \tan^{-1} \frac{y}{x}, \text{ therefore, one gets:} \\ I &= \frac{n_0 \Delta}{r_c^\alpha} \int_0^{\sqrt{r_c^2 - x^2}} (x^2 + y^2)^{\frac{\alpha}{2}} dy = \frac{n_0 \Delta}{r_c^\alpha} \int_0^\theta (x^2 + x^2 \tan^2 \theta)^{\frac{\alpha}{2}} x \sec^2 \theta d\theta \\ &= \frac{n_0 \Delta}{r_c^\alpha} \int_0^{\tan^{-1} \frac{\sqrt{r_c^2 - x^2}}{x}} x^{\alpha+1} (1 + \tan^2 \theta)^{\frac{\alpha}{2}} \sec^2 \theta d\theta \quad (8) \end{aligned}$$

By using the trigonometric identity, $(1 + \tan^2 \theta) = (\sec^2 \theta)$, Eq. (8) can be written as:

$$I = \frac{n_0 \Delta}{r_c^\alpha} \int_0^{\tan^{-1} \frac{\sqrt{r_c^2 - x^2}}{x}} x^{\alpha+1} (\sec \theta)^{\alpha+2} d\theta$$

The value of I can be obtained by using integration by parts and after some manipulations its value is given by:

$$I = n_0 \Delta \frac{\sqrt{r_c^2 - x^2}}{(\alpha+1)} \left\{ 1 + \frac{\alpha}{(\alpha-1)} \frac{x^2}{r_c^2} + \frac{\alpha(\alpha-2)}{(\alpha-1)(\alpha-3)} \frac{x^4}{r_c^4} + \frac{\alpha(\alpha-2)(\alpha-4)}{(\alpha-1)(\alpha-3)(\alpha-5)} \frac{x^6}{r_c^6} + \dots + \frac{\alpha(\alpha-2)(\alpha-4)\dots(\alpha-(n-2))}{(\alpha-1)(\alpha-3)(\alpha-5)\dots(\alpha-(n-1))} \frac{x^n}{r_c^n} \right\} \quad (9)$$

When even values of α are considered in eq. (9), then terms taken into consideration are those which are not vanishing for the given value of α . In case of odd α -values, terms which give infinity for a given value of α are omitted and the value $n_0 \Delta \left(\frac{x^{\alpha+1}}{r_c^\alpha} \right) \frac{(\alpha+1)!}{2^{\alpha+1} \left(\frac{\alpha+1}{2} \right)!} \log \left(\frac{r_c + \sqrt{y^2 - x^2}}{x} \right)$ is added outside the bracket.

Substituting from (6) and (9) into (5), one gets:

$$\begin{aligned} \frac{\lambda}{2} \frac{dZ}{dZ} &= (n_{cl} - n_L) \sqrt{r_f^2 - x^2} - n_{cl} \sqrt{r_c^2 - x^2} + n_o \sqrt{r_c^2 - x^2} - \\ &n_o \Delta \frac{\sqrt{r_c^2 - x^2}}{(\alpha+1)} \left\{ 1 + \frac{\alpha}{(\alpha-1)} \frac{x^2}{r_c^2} + \frac{\alpha(\alpha-2)}{(\alpha-1)(\alpha-3)} \frac{x^4}{r_c^4} + \frac{\alpha(\alpha-2)(\alpha-4)}{(\alpha-1)(\alpha-3)(\alpha-5)} \frac{x^6}{r_c^6} + \dots \frac{\alpha(\alpha-2)(\alpha-4)\dots(\alpha-(n-2))}{(\alpha-1)(\alpha-3)(\alpha-5)\dots(\alpha-(n-1))} \frac{x^n}{r_c^n} \right\} \quad (10) \end{aligned}$$

Eq. (11) can be rewritten in the form:

$$\begin{aligned} \frac{\lambda}{2} \frac{dZ}{dZ} &= (n_{cl} - n_L) \sqrt{r_f^2 - x^2} + (n_o - n_{cl}) \sqrt{r_c^2 - x^2} - \frac{\alpha}{\alpha+1} \left[1 - \left\{ \frac{1}{\alpha-1} \frac{x^2}{r_c^2} + \frac{\alpha-2}{(\alpha-1)(\alpha-3)} \frac{x^4}{r_c^4} + \frac{(\alpha-2)(\alpha-4)}{(\alpha-1)(\alpha-3)(\alpha-5)} \frac{x^6}{r_c^6} + \dots \frac{\alpha(\alpha-2)(\alpha-4)\dots(\alpha-(n-2))}{(\alpha-1)(\alpha-3)(\alpha-5)\dots(\alpha-(n-1))} \frac{x^n}{r_c^n} \right\} \right] \quad (11) \end{aligned}$$

3 Experimental Technique

3.1 Phase-shifting interferometry

Phase-shifting interferometry has been shown to be a powerful method for measuring the refractive index profiles of optical and synthetic fibers [15-16]. Well known advantages of phase shifting interferometry over conventional interferometers include: (1) high measurement accuracy, (2) rapid measurements, (3) good results even with low contrast fringes and (4) phase obtained at a grid of data points [22]. When two beams that originate from a common light source are recombined after they have travelled optical paths that differ by no more than the coherence length of the source, they interfere and form a fringe pattern. This is usually recorded with a 2D detector array and can be described by the following intensity distribution,

$$I_i(x, y) = I_0(x, y) + I_M(x, y) \cos[\varphi(x, y) + \Delta\varphi_i] \quad (12)$$

where $I_0(x, y)$, $I_M(x, y)$, $\varphi(x, y)$ are three unknown distributions referred to as the background intensity, the modulation intensity and the phase difference between the interfering beams, respectively, and x and y are spatial coordinates. $\Delta\varphi_i$ is a known phase shift introduced between the interfering beams.

In order to evaluate the phase, $\varphi(x, y)$, at least three independent measurements of the intensity $I_i(x, y)$ are required. Four-frame algorithm, a simple and widely used phase evaluation algorithm [23-24], is used to evaluate the phase distribution. It is based on recording four intensity measurements I_1, I_2, I_3 and I_4 at $\Delta\varphi_i = 0, \pi/2, \pi, 3\pi/2$ radians phase shifts, respectively.

Under the assumption that $\varphi(x, y)$ does not change during the acquisition of I_1 to I_4 , it can be shown that [25]

$$\varphi_w(x, y) = \tan^{-1} \left(\frac{I_4(x, y) - I_2(x, y)}{I_1(x, y) - I_3(x, y)} \right) \quad (13)$$

The arctangent function, $\varphi_w(x, y)$ is wrapped between $+\pi$ and $-\pi$ is referred to as the wrapped phase. The process of recovering the continuous phase distribution $\varphi(x, y)$ that extends between $-\pi$ radians and $+\pi$ radians is known as phase unwrapping, and consists of adding an appropriate integer multiple of 2π at each point in the wrapped phase distribution [23, 26-30]. The relation between the measured unwrapped phase distribution $\varphi(x, y)$ and the spatial varying optical path length difference, $\delta OPL(x, y)$, is given by the relation [17]

$$\delta OPL(x, y) = \frac{\lambda}{2\pi} \varphi(x, y) \quad (14)$$

3.2 Experimental set-up

Fig. 2 shows a schematic of phase-shifting Mach-Zehnder interferometer. A He-Ne laser is used as the coherent light source, providing a beam with wavelength $\lambda = 632.8$ nm. The beam was spatially filtered by spatial filter (SF) and then collimated by lens (L1). A non-polarizing beam splitter (NPBS1) divides the incoming collimated beam into a collimated reference beam (RB) and a collimated object beam (OB). The collimated reference beam (RB) is reflected by the mirror M1, which is mounted on an open loop piezoelectric lead zirconatetitanate (PZT) transducer. The PZT actuator is a Physik Instrument type PL055.30 PZT which is a low voltage device with a maximum displacement of $2.2 \mu\text{m}$ for 100 V of applied voltage. The PZT is used to controllably shift the phase of the reference beam by introducing controlled $\pi/2$ phase difference between two successive interferograms. The collimated object beam (OB) is reflected from mirror M2 and illuminates the fiber, which magnified by a microscope objective lens (MO2) with magnification $10\times$ and N.A. 0.25. In order to compensate the wavefront of the object beam, a typical microscope objective lens (MO1) is placed in the reference arm.

The fiber is held vertically, to the observation direction, in a liquid cell (LC) containing a liquid of refractive index n_L quite close to the cladding refractive index. The collimated object beam is recombined with the reference beam at the second non-polarizing beam splitter (NPBS2). A CMOS camera (C) records four phase shifted interferograms formed by the interference between the reference and object beams. These interferograms are stored on the computer storage media and automatically processed to generate the wrapped phase map of the fringe pattern using eq. (13). The camera is a 1280×1024 pixels, 8 bits, black and white, with square pixels of $5.2 \mu\text{m}$, and a maximal frame rate up to 25Hz.

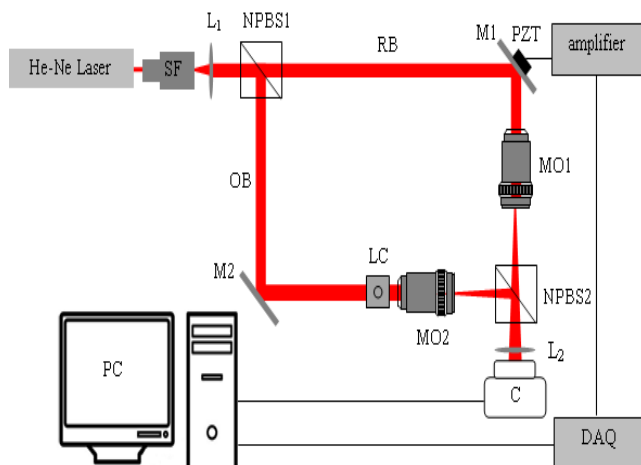


Fig. 2. Schematic of phase-shifting Mach-Zehnder interferometer: SP, Spatial filter; NPBS1 and NPBS2, non-polarizing beam splitters; M1 and M2, mirrors; PZT, open loop piezoelectric transducer; RB, reference beam; OB, object beam; MO1 and MO2, microscopic objective lenses;

LC, liquid cell; L2, imaging lens; DAQ, digital to analogue converter; C, camera.

4 Experimental Measurements and Theoretical Calculations

4.1 δOPL measurements using phase shifting interferometry

The aim of using phase shifting Mach-Zehnder interferometry is to provide the proposed model with the δOPL profile across the GRIN optical fiber sample. To achieve this, four-frame algorithm was employed to obtain the phase distribution across the sample and then convert the phase distribution into δOPL using Eq. (14). As mentioned in Section 3.1, the four-frame algorithm requires the acquisition of four interferograms with $\pi/2$ phase shifts between successive ones. The displacement/voltage response of the PZT actuator, used to shift the phase of the RB, is sensitive to environmental vibrations and changes in humidity and temperature. For this reason, they need to be calibrated before each measurement and to determine the voltage values that are required to introduce $\pi/2$ phase steps. The procedure described by Ochoa et al [30] was followed to calibrate the PZT phase shifting actuator. The procedure is only suitable for calibrating phase modulators that can produce a full 2π phase shift and for which the phase changes monotonically with applied voltage, but is relatively simple to implement and can be performed in situ. Four interferograms obtained with $0, \pi/2, \pi, 3\pi/2$ phase shifts are shown in Fig. 3. The fiber sample was a multimode GRIN optical fiber (GIF625-Thorlabs). According to the supplier, the core diameter is $62.5 \pm 2.5 \mu\text{m}$ and the cladding diameter is $125 \pm 1 \mu\text{m}$.

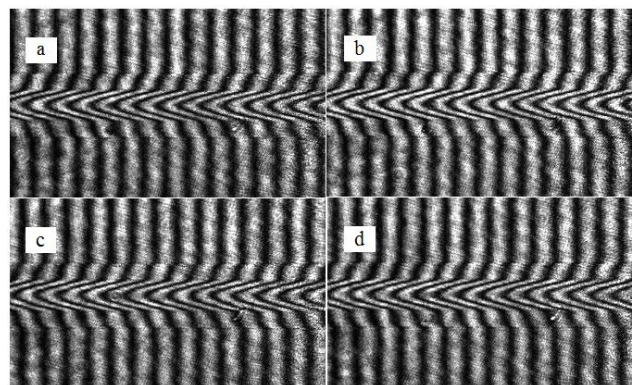


Fig. 3. Phase shifted interferograms of GRIN optical fiber immersed in liquid of refractive index $n_L = 1.4575$ with additional phase (a) 0 , (b) $\frac{\pi}{2}$, (c) π and (d) $\frac{3\pi}{2}$ phase difference.

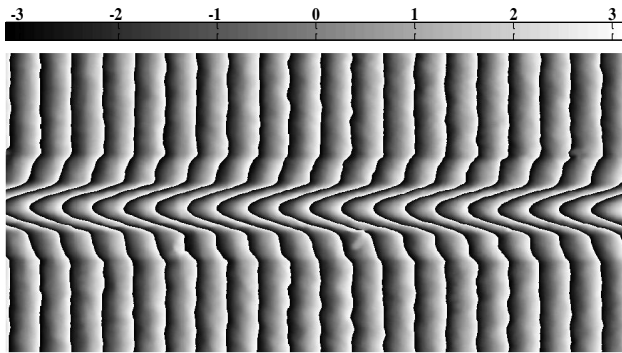


Fig. 4. Wrapped phase distribution, $\phi_w(x, y)$, for GRIN optical fiber (color bar in radians).

The sample was immersed in a suitable liquid, mixture of butyl stearate and paraffin oil, with a refractive index quite close to the cladding refractive index, $n_L = 1.4575$ at 21°C . An Abbe refractometer, with an accuracy of ± 0.0001 , was used to measure the refractive index of the immersion liquid. These interferograms were combined, using Eq. 13, to extract the wrapped phase distribution, $\phi_w(x, y)$, across the sample relative to the surrounding medium. Fig. 4 shows typical results of $\phi_w(x, y)$ for GRIN optical fiber. As can be seen in Fig. 4, the wrapped phase distribution lie in the range $(-\pi, \pi)$. The changing in color discontinuously from white to black means there is a phase jump of 2π . In this work, the unwrapped phase distribution, $\phi(x, y)$, were obtained, as shown in Fig. 5, with the use of Goldstein branch cut phase unwrapping algorithm [31]. It can be seen that the 2π discontinuities have been removed by adding an appropriate integer multiple of 2π at each point in the wrapped phase distribution. Having obtained the unwrapped phase distribution, the δOPL and hence the mean fringe shift across sample can be evaluated, shown in Fig. 6, using the relation [17]

$$\delta OPL = \frac{\lambda dZ}{\Delta Z} = \frac{\lambda}{2\pi} \phi(x, y)$$

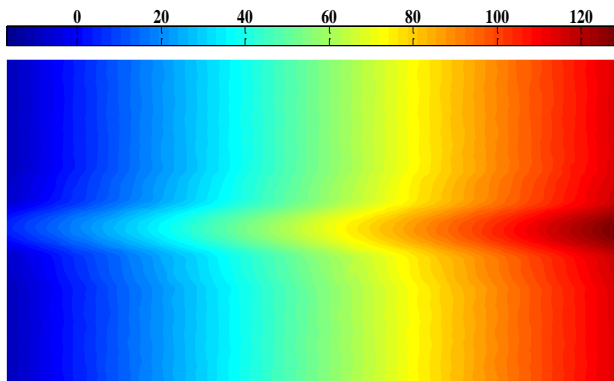


Fig. 5. Unwrapped phase distribution, $\phi(x, y)$ for GRIN optical fiber (color bar in radians).

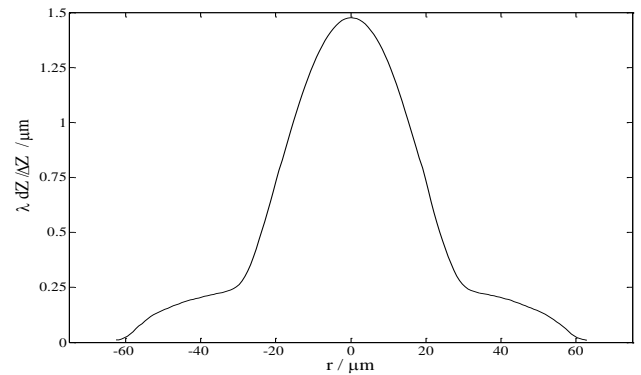


Fig. 6. Mean fringe shift across the GRIN optical fiber.

4.2 Numerical evaluation of the core/cladding refractive indices of GRIN optical fiber

The cladding refractive index of GRIN optical fiber was measured with the aid of the two beam interferograms. The interferograms and measurement is shown in Fig. 6. The measurements were achieved from the following equation which determines the ratio between the fringe shift dZ to the fringe spacing ΔZ within the cladding layer:

$$\frac{\lambda dZ}{2 \Delta Z} = (n_{cl} - n_L) \sqrt{r_f^2 - x^2} \quad , r_c \leq x \leq r_f \quad (15)$$

Substituting for the values of n_L and $\frac{\lambda dZ}{2 \Delta Z}$ at arbitrary chosen x -value from the experimental results as shown in (Fig. 6) and eq. (15), the measured results r_c , r_f and n_{cl} of the GRIN optical fiber are in table 1.

Table 1: Measured GRIN optical fiber parameters

| n_L | λ (nm) | r_c (μm) | r_f (μm) | n_{cl} (μm) |
|--------|----------------|-------------------------|-------------------------|----------------------------|
| 1.4575 | 633 | 31 | 62.5 | 1.4597 |

In the following section we show the measurements of the peak value of the fiber core n_0 and extraction of the profile shape parameter α . Equation (11) was solved for the two unknowns (n_0 & α) by putting ($x = 0$ and $x = \frac{1}{2}r_c$ and/or $x = \frac{1}{4}r_c$), see (Fig. 6). At ($x=0$) equation (11) becomes:

$$(n_0 - n_{cl}) = \left[\frac{\lambda dZ}{2 \Delta Z} - (n_{cl} - n_L)r_f \right] \left(\frac{\alpha+1}{\alpha} \right) \frac{1}{r_c} \quad (16)$$

Substituting in eq. (11) with the values in table 1 and the measured $\left(\frac{dZ}{\Delta Z}\right)$ at ($x=0$) one gets:

$$(n_0 - n_{cl}) = 0.01937 \left(\frac{\alpha+1}{\alpha} \right) \quad (18)$$

Also putting ($x = \frac{1}{4}r_c$) one gets using eq. (11)

$$\alpha^4(0.0511) - \alpha^3(0.21313) - \alpha^2(0.06549) + \alpha(0.3297) = 0 \quad (18)$$

This gives a fourth order equation of one variable α . The solution of eq.(18) gives four α roots; $\alpha = 0, -1, 2.1035$ and 3.0763 . The root $\alpha=0$ means no core refractive index distribution, $\alpha=-1$ and $\alpha=3.0763$ give odd symmetric

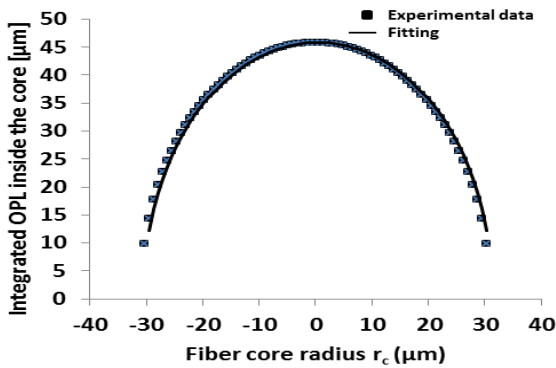
profile, then $\alpha=2.1035$ is the solution which gives an even symmetric profile with respect to the center point of the fiber. By substituting for $\alpha=2.1035$ in eq. (16) one gets $n_0=1.4885$. The obtained value of n_0 is exactly agreed with the published values for the same GRIN optical fiber [18] despite different manufacturer.

4.3 Model validation

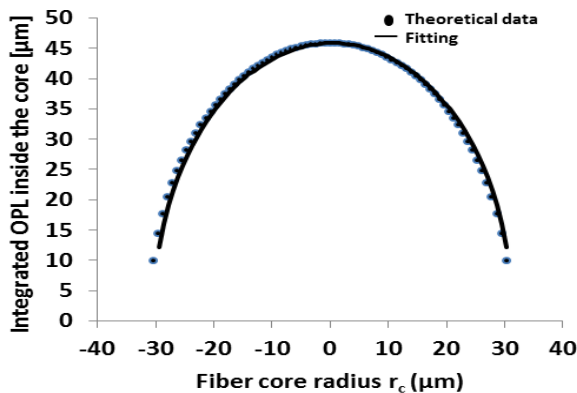
Equation (10) can be written in the form of two equal parts $F(x)$ as follows:

$$\frac{\lambda}{2\Delta z} - (n_{cl} - n_L) \sqrt{r_f^2 - x^2} + n_{cl} \sqrt{r_c^2 - x^2} = n_0 \sqrt{r_c^2 - x^2} - (n_0 - n_{cl}) \frac{\sqrt{r_c^2 - x^2}}{\alpha + 1} \left\{ 1 + \frac{\alpha}{\alpha - 1} \frac{x^2}{r_c^2} + \frac{\alpha(\alpha - 2)}{(\alpha - 1)(\alpha - 3)} \frac{x^4}{r_c^4} \right\} = F(x) \quad (19)$$

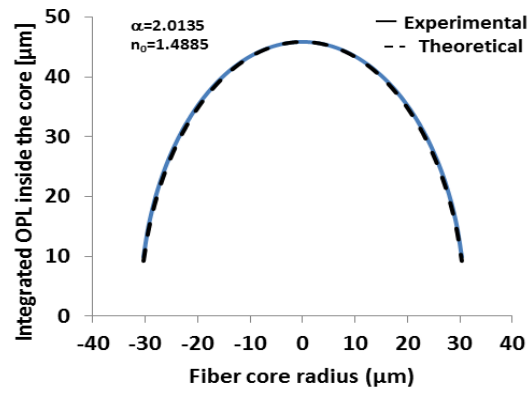
The left hand side part gives $F(x)$ using the experimental measurements of $\left(\frac{dz}{dz}\right)$ while the right hand side represents $F(x)$ through the theoretical integration of the optical path length crossing the GRIN fiber core. It represents the integrated optical path length crossing the fiber parallel to the Y-axis as a function of x - in the range of the fiber core thickness.



(a)



(b)



(c)

Fig. 7. (a) The experimental measurements of OPL inside the fiber core by using eq. (19) (b) theoretical calculations and (c) comparison between theoretical calculations and experimental results.

Using the experimental measurements of $\left(\frac{dz}{dz}\right)$ as a function of x and the measured value of $n_{cl}=1.4597$, $n_L=1.4575$, $r_f=62.5 \mu\text{m}$ and $r_c=31 \mu\text{m}$, best fitting between the left hand side part experimentally measured and the right hand side theoretically derived for $\alpha=2.1035$ and $n_0=1.885$ as shown in Fig. 7(c) is obtained. The fitting is represented in the range $-r_c \leq x \leq r_c$ of the GRIN optical fiber core thickness where the theoretical derivation is carried out.

5 Conclusion

A new mathematical model for GRIN optical fibers was developed. The mathematics treated the fiber core as a single layer and can be used directly to measure and configure the refractive index profile of GRIN optical fibers. With this model one can obtain exact and accurate propagation parameters of the used GRIN optical fibers. The model is applicable for any α -shape parameter. The theoretical calculations were validated experimentally using high precision phase-shifting interferometry. The experimental results were coinciding with theoretical calculations.

Acknowledgement

The authors would like to express their gratitude to Prof. Dr. M. M. EL-Nicklawy for his generous help for producing this work. Also authors would like to acknowledge Prof. Dr. A. F. Hassan for the fruitful discussion.

References

- [1] G. E. Agrawal, *Optic Communication Systems*, Institute of optics 3rd ed. (Wiley& Sons, Inc 2002).
- [2] S. Yin, P. B. Ruffin and F. T. S. Yu, *Fiber Optic Sensors*, 2nd ed. (CRC press 2008).

- [3] F. J. Dignonnet, *Rare Earth Doped Fiber Lasers and Amplifiers* 2nd ed. (Dekker, New York 2001).
- [4] R. M. El-Agmy, *Laser Phys.* **18**, 803 (2008).
- [5] R. M. El-Agmy and N. M. Al-Hosiny, *Laser Phys.* **20**, 838 (2010).
- [6] R. M. El-Agmy, W. Lüthy, Th. Graf and H. P. Weber, *Electronics letters* **39**, 507 (2003).
- [7] B. E. A. Saleh, *Fundamentals of Photonics*, 2nd ed. (Hoboken-NJ 2007).
- [8] R. P. Khare, *Fiber Optics and Optoelectronics* (Oxford University Press 2004).
- [9] P. Ivan Kaminow and Li. Tingye Optical, *Fiber Telecommunications IV-A* 4th. ed. (Academic Press 2002).
- [10] C. Manolatu and H. A. Haus, *Passive Components for Dense Optical Integration* (Kluwer academic publishers 2002).
- [11] N. Barakat and A.A. Hamza, *Interferometry of Fibrous Materials*. (Adam Hilger UK 1990).
- [12] M. M. El-Nicklawy, I. M. Fouda, *J. Text. Inst.* **5**, 252 (1980).
- [13] M. EL-Nicklawy, I. M. Fouda, and A. F. Hassan, *Polymer Testing* **16**, 33 (1997).
- [14] I. M. Fouda, M. M. El-Nicklawy, A. F. Hassan, A. M. Kelany. *Polymer International* **38**, 233 (1995).
- [15] H.H. Wahba, Th. Kreis, *J. Opt. A: Pure Appl. Opt.* **11**, 105407 (2009).
- [16] K. M. Yassien and M. El Bakary, *Optics and Photonics Journal* **4**, 153 (2014).
- [17] H. H. Wahba and T. Kreis, *Appl. Opt.* **48**, 1573 (2009).
- [18] M. A. Shams El-Din and H. H. Wahba, *Opt. Comm.* **284**, 3846 (2011).
- [19] H. H. Wahba and Th Kreis *SPIE Proc.* **7389**, 73890K (2009).
- [20] K. Yassien, M. Agour, C.V. Koyplow, H. Dessouky, *Opt. and Lasers Eng.* **48**, 555 (2010).
- [21] A. A. Hamzat, T. Z. N. Sokkart, A. M. Ghandarf, M. A. Mabroukf, W A Ramadant *Pure Appl. Opt.* **4**, 161 (1995)
- [22] Y. Y. Cheng, and J. C. Wyant, *Appl. Opt.* **24** (18), 3049 (1985).
- [23] J. M. Huntley, *Automated Analysis of Speckle Interferograms. In Digital Speckle Pattern Interferometry and Related Techniques* 2nd ed. (John Wiley & Sons Ltd. 2001)
- [24] C. Wei, M. Chen, Z. Wang, *Opt. Eng.* **38** (8), 1357 (1999).
- [25] K. Creath, In E, *Progress in Optics* Wolf ed. (New York Elsevier 1988).
- [26] J. M. Huntley, *Appl. Opt.* **28** (15), 3268 (1989).
- [27] T. R. Judge and P. J. Bryanston-Cross, *Opt. Lasers Eng.* **21**, 199 (1994).
- [28] D. Kerr, G. H. Kaufmann and G. E. Galizzi., *Appl. Opt.* **35** (5), 810 (1996).
- [29] A. Ochoa and J. M. Huntley, *Opt. Eng.* **37** (9), 2501 (1998).
- [30] D. C. Ghiglia and M. D. Pritt, *Two-Dimensional Phase Unwrapping: Theory, Algorithms and Software* (New York: Wiley-Interscience 1998).
- [31] R. M. Goldstein, H. A. Zebken, and C. L. Werner, *Radio Sci.* **23** (4), 713 (1988).
-